JOURNAL OF SPACECRAFT AND ROCKETS
Vol. 39, No. 1, January–February 2002

Determining Angular Velocity and Angular Acceleration of Projectiles Using Triaxial Acceleration Measurements

Mark Costello* and Thanat Jitpraphai†
Oregon State University, Corvallis, Oregon 97331

Estimation of body frame components of angular velocity and angular acceleration of a projectile undergoing general three-dimensional motion using linear acceleration measurements is considered. For the case where triaxial components of linear acceleration are known at three noncolinear points, the kinematic equations must in general be transformed to a computational plane before a useful solution is obtained. However, when more than three point measurements are utilized, a solution is obtained without the need to transform the kinematic equations to a computational plane. The sensitivity of angular rates to measurement errors is a nonlinear function of angular rates and sensor geometry. For a body that nutates and precesses as it rolls, large errors can be induced for some combinations of angular rates and sensor configurations. However, utilization of acceleration measurements at many points on the skin of an atmospheric rocket can effectively estimate the angular rates and accelerations with noisy, quantized acceleration measurements.

Nomenclature

A	=	relative acceleration matrix
$\tilde{a}_{X_i}, \tilde{a}_{Y_i}, \tilde{a}_{Z_i}$	=	components of acceleration of the ith accelerometer in the computational frame
B	=	body reference frame
C	=	computational frame
G	=	sensitivity matrix
I	=	inertial reference frame
$\boldsymbol{i}_B, \boldsymbol{j}_B, \boldsymbol{k}_B$	=	unit vectors of the body reference frame
$\boldsymbol{i}_C, \boldsymbol{j}_C, \boldsymbol{k}_C$	=	unit vectors of the computational plane
M	=	matrix contains angular velocities and angular acceleration in the computational plane
p, q, r	=	components of the angular velocity vector of the projectile in the B frame
$\tilde{p}, \tilde{q}, \tilde{r}$	=	components of estimated angular rate in the computational plane
$\hat{p}, \hat{q}, \hat{r}$	=	components of noisy estimated angular rate in the computational plane
R	=	relative position matrix of sensors in the computational plane
$\boldsymbol{r}_{\varphi \to \beta}$	=	distance vector from φ to β in B frame
$\boldsymbol{U}$	=	algorithm input acceleration components
$\tilde{x}_1, \tilde{x}_2, \tilde{y}$	=	geometric distance of the computational plane
$\boldsymbol{Y}$	=	algorithm angular rate and angular acceleration components
$\boldsymbol{\alpha}_{B/I}$	=	angular acceleration of the body reference frame with respect to the inertial reference frame
$\tilde{\alpha}_x, \tilde{\alpha}_y, \tilde{\alpha}_z$	=	components of estimated angular acceleration in the computational plane
φ, β, χ	=	sensor points on the body
$\boldsymbol{\omega}_{B/I}$	=	angular velocity of the body reference frame with respect to the I frame

Introduction

SMALL and rugged microelectromechanical sensors (MEMS) offer the potential to implement active flight control systems onboard medium- and even small-caliber projectiles. A wide variety of sensor technologies are being explored, such as linear accelerometers, magnetic roll sensors, tuning fork gyroscopes, magnetohydrodynamic angular rate sensors, and diaphragm strain gauge surface pressure sensors, to name a few.[1–3] Several studies have been conducted regarding potential performance improvements in large-, medium-, and small-caliber projectiles that utilize some form of an active flight control system.[4–6] The potential performance enhancements are indeed impressive. However, for practical design implementation, the sensors must be small and highly cost competitive so that the sensor suite does not dominate the cost of the entire projectile, which is of course a one-time use item. Although MEMS technology is rapidly changing with innovative sensor configurations regularly entering the market, currently linear accelerometers are by far the least expensive and most developed devices.

Rigid-body kinematics provides a link between linear acceleration, angular velocity, and angular acceleration. Because angular velocity and angular acceleration are body properties and linear acceleration is a point property,[7] the linear acceleration at several points on a rigid body can be used to compute the angular velocity and acceleration of a body. Several algorithms have been developed for different applications. For example, Padgaonkar et al.[8] used nine single-axis acceleration measurements at four different noncoplanar points to compute angular velocity and acceleration components. Genin et al.[9] showed that the minimum number of acceleration measurements needed to estimate both angular velocity and acceleration is nine. Harkins and Brown[10] explored the use of four single-axis linear accelerometers aligned with the body axis of a projectile to compute angular velocity and acceleration. When applied to a direct fire atmospheric rocket, digital accelerometer output at 16-B resolution was necessary. Clusters of three, triaxial-axis accelerometers have also been proposed to compute the angular rates and accelerations. A method developed by Angeles[11] computes the angular velocity and acceleration of a body by exploiting the properties of skew symmetric matrices. The linear acceleration data are numerically integrated to obtain necessary linear velocity information. Another method due to Nusholtz[12] is based on spherical geometric analysis. When the properties of acceleration components on a sphere are used, the method determines both angular velocity and angular acceleration with three triaxial accelerometers. This technique also relies on numerical integration, as well as numerical differentiation.

The work reported here develops a general technique to estimate body frame components of angular velocity and acceleration of a rigid body using triaxial acceleration measurements that are free from numerical integration or differentiation. An error analysis is conducted to establish how acceleration measurements errors propagate into angular rate estimation errors. When a realistic direct fire

Received 10 August 2000; revision received 3 September 2001; accepted for publication 11 September 2001.

*Assistant Professor, Department of Mechanical Engineering. Member AIAA.
†Graduate Research Assistant, Department of Mechanical Engineering.

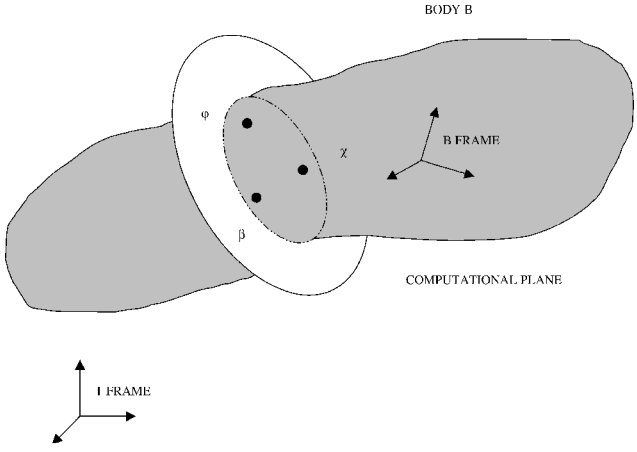

Fig. 1 General sensor configuration.

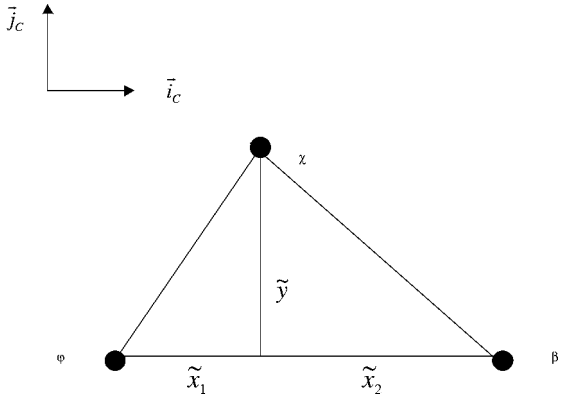

Fig. 2 Computational plane geometry.

atmospheric rocket trajectory is used, angular rates and accelerations are estimated with clusters of accelerometers placed on the skin of the rocket. Practical issues such as the required number of sensors, sensor arrangement, data fusion, and quantization errors are addressed.

Three Triaxial Accelerometers Clusters

The minimum number of sensors to measure both angular rate and angular acceleration components of a body using linear acceleration measurement is three.[9] Consider Fig. 1, which shows three triaxial accelerometers mounted arbitrarily on a rigid body along with the different reference frames used in the analysis. The accelerometers are located at points φ, β, and χ. The computational plane is defined as the plane formed by the sensor location points φ, β, and χ. The computational frame C is aligned with the computational plane but is collocated with the body reference frame B. Figure 2 details the geometry of the computational plane. It is assumed that the position and orientation of each sensor are known in the body frame. When these data are used, the unit vectors of the computational frame are determined. The unit vector $\boldsymbol{i}_C$ is parallel to the distance vector from φ to β, whereas the $\boldsymbol{k}_C$ axis is perpendicular to the computational plane and the unit vector $\boldsymbol{j}_C$ completes the right-handed triad. When these definitions are used, an orthogonal transformation from the body frame to the computational frame can be formed. The difference in the linear acceleration of two points fixed on a rotating body B with respect to an inertial reference frame I is given by

$$\boldsymbol{a}_{\beta/I} - \boldsymbol{a}_{\varphi/I} = \boldsymbol{\alpha}_{B/I} \times \boldsymbol{r}_{\varphi\to\beta} + \boldsymbol{\omega}_{B/I} \times (\boldsymbol{\omega}_{B/I} \times \boldsymbol{r}_{\varphi\to\beta}) \quad (1)$$

where $\boldsymbol{\alpha}_{B/I}$ is the angular acceleration of B with respect to I, $\boldsymbol{\omega}_{B/I}$ is the angular velocity of B with respect to I, and $\boldsymbol{r}_{\varphi\to\beta}$ is the distance vector from φ to β. Measure numbers with a tilde refer to the computation frame, whereas those without refer to the body frame. Application of Eq. (1) to body point combinations φ–β, φ–χ, and β–χ generates three sets of equations that are concatenated into matrix form as

$$A = MR \quad (2)$$

$$A = \begin{bmatrix} \tilde{a}_{X_\beta} - \tilde{a}_{X_\varphi} & \tilde{a}_{X_\chi} - \tilde{a}_{X_\varphi} & \tilde{a}_{X_\chi} - \tilde{a}_{X_\beta} \\ \tilde{a}_{Y_\beta} - \tilde{a}_{Y_\varphi} & \tilde{a}_{Y_\chi} - \tilde{a}_{Y_\varphi} & \tilde{a}_{Y_\chi} - \tilde{a}_{Y_\beta} \\ \tilde{a}_{Z_\beta} - \tilde{a}_{Z_\varphi} & \tilde{a}_{Z_\chi} - \tilde{a}_{Z_\varphi} & \tilde{a}_{Z_\chi} - \tilde{a}_{Z_\beta} \end{bmatrix} \quad (3)$$

$$M = \begin{bmatrix} -\tilde{q}^2 - \tilde{r}^2 & -\tilde{\alpha}_Z + \tilde{p}\tilde{q} & \tilde{\alpha}_Y + \tilde{p}\tilde{r} \\ \tilde{\alpha}_Z + \tilde{p}\tilde{q} & -\tilde{p}^2 - \tilde{r}^2 & -\tilde{\alpha}_X + \tilde{q}\tilde{r} \\ -\tilde{\alpha}_Y + \tilde{p}\tilde{r} & \tilde{\alpha}_X + \tilde{q}\tilde{r} & -\tilde{p}^2 - \tilde{q}^2 \end{bmatrix} \quad (4)$$

$$R = \begin{bmatrix} \tilde{x}_1 + \tilde{x}_2 & \tilde{x}_1 & -\tilde{x}_2 \\ 0 & \tilde{y} & \tilde{y} \\ 0 & 0 & 0 \end{bmatrix} \quad (5)$$

Unfortunately, the distance matrix R is singular because any two of the three distance vectors can be either added or subtracted to obtain the third vector. For three noncollinear points, the distance matrix has rank two. If the kinematic equations are written in the computational frame as shown earlier, the generalized inverse allows the first two columns of M to be reconstructed:

$$RR^{-1} = \begin{bmatrix} 1 & 0 & 0 \\ 0 & 1 & 0 \\ 0 & 0 & 0 \end{bmatrix} \quad (6)$$

The property given in Eq. (6) is not unique to the computational frame as already defined. Any computational frame with one axis perpendicular to the plane formed by the three sensor points will permit two of the columns of M to be reconstructed. Multiplication of Eq. (2) by R^{-1} yields

$$AR^{-1} = \begin{bmatrix} M_{1,1} & M_{1,2} & 0 \\ M_{2,1} & M_{2,2} & 0 \\ M_{3,1} & M_{3,2} & 0 \end{bmatrix} \quad (7)$$

Using sensor position and acceleration measurement data, Eq. (7) provides a method to compute the first two columns of the matrix of unknowns, M, and as such furnishes six equations. Whereas M consists of nine elements, the matrix is generated with six parameters that appear in a nonlinear manner. The solution of these equations is given by

$$\tilde{p} = s_{\tilde{p}}\sqrt{\tfrac{1}{2}\left[(M_{1,1} - M_{2,2}) + \sqrt{(M_{1,1} - M_{2,2})^2 + (M_{1,2} + M_{2,1})^2}\right]} \quad (8)$$

$$\tilde{q} = s_{\tilde{q}}\sqrt{\tfrac{1}{2}\left[(M_{2,2} - M_{1,1}) + \sqrt{(M_{1,1} - M_{2,2})^2 + (M_{1,2} + M_{2,1})^2}\right]} \quad (9)$$

$$\tilde{r} = s_{\tilde{r}}\sqrt{-\tfrac{1}{2}\left[(M_{1,1} + M_{2,2}) + \sqrt{(M_{1,1} - M_{2,2})^2 + (M_{1,2} + M_{2,1})^2}\right]} \quad (10)$$

$$\tilde{\alpha}_X = -s_{\tilde{q}}s_{\tilde{r}}\sqrt{-\tfrac{1}{4}(M_{1,2} + M_{2,1})^2 - \tfrac{1}{2}M_{2,2}\left(M_{2,2} - M_{1,1} + \sqrt{(M_{1,1} - M_{2,2})^2 + (M_{1,2} + M_{2,1})^2}\right)} + M_{3,2} \quad (11)$$

$$\tilde{\alpha}_Y = s_{\tilde{p}}s_{\tilde{r}}\sqrt{-\tfrac{1}{4}(M_{1,2} + M_{2,1})^2 - \tfrac{1}{2}M_{1,1}\left(M_{1,1} - M_{2,2} + \sqrt{(M_{1,1} - M_{2,2})^2 + (M_{1,2} + M_{2,1})^2}\right)} - M_{3,1} \quad (12)$$

$$\tilde{\alpha}_Z = \tfrac{1}{2}(M_{2,1} - M_{1,2}) \tag{13}$$

In Eqs. (8–12), $s_{\tilde{p}}$, $s_{\tilde{q}}$, and $s_{\tilde{r}}$ are the algebraic signs of $\tilde{p}$, $\tilde{q}$, and $\tilde{r}$, respectively. The kinematic formulas cannot isolate the algebraic signs of $\tilde{p}$, $\tilde{q}$, and $\tilde{r}$. To see this, note that if $\tilde{p}$, $\tilde{q}$, and $\tilde{r}$ is a solution to Eq. (2), then $-\tilde{p}$, $-\tilde{q}$, and $-\tilde{r}$ must also be a solution because the M matrix is identical in both cases. Thus, two valid solutions to this inverse problem exist.

More Than Three Triaxial Accelerometers Clusters

When more than three noncoplanar triaxial accelerometers are employed, there is no need to transform the geometric and measurement data to a computational plane because the distance matrix R is full rank. The distance matrix will be full rank provided at least four of the points in the sensor cluster are noncoplanar. In this case, all three columns of M can be completely reconstructed directly in the body frame. If n body point combinations are generated, then application of Eq. (1) generates n columns of data in the acceleration matrix A and the distance matrix R. The solution formulas are provided as

$$p = s_p\sqrt{\tfrac{1}{2}\left[(M_{1,1} - M_{2,2}) + \sqrt{(M_{1,1} - M_{2,2})^2 + (M_{1,2} + M_{2,1})^2}\right]} \tag{14}$$

$$q = s_q\sqrt{\tfrac{1}{2}\left[(M_{2,2} - M_{1,1}) + \sqrt{(M_{1,1} - M_{2,2})^2 + (M_{1,2} + M_{2,1})^2}\right]} \tag{15}$$

$$r = s_r\sqrt{-\tfrac{1}{2}\left[(M_{1,1} + M_{2,2}) + \sqrt{(M_{1,1} - M_{2,2})^2 + (M_{1,2} + M_{2,1})^2}\right]} \tag{16}$$

$$\alpha_X = \tfrac{1}{2}(M_{3,2} - M_{2,3}) \tag{17}$$

$$\alpha_Y = \tfrac{1}{2}(M_{1,3} - M_{3,1}) \tag{18}$$

$$\alpha_Z = \tfrac{1}{2}(M_{2,1} - M_{1,2}) \tag{19}$$

As with the three-triaxial-cluster case, two valid solutions are possible depending on the algebraic sign of p, q, and r. Notice that the angular acceleration components can be directly computed without knowledge of the algebraic sign of the angular velocity components, whereas in the three-point case, α_X and α_Y required knowledge of the algebraic sign.

Algebraic Sign Determination

Success of both estimation algorithms discussed fundamentally relies on knowledge of the algebraic sign of the angular velocity components. Regrettably, Eq. (2) has no means to distinguish between the two possible solutions. Additional auxiliary information must be introduced for this specific purpose. For sensor clusters using more than three noncoplanar points, knowledge of the algebraic sign of one of the angular velocity components is sufficient to establish the remaining algebraic signs. In a practical setting, this is often the case because gun rifling or projectile fin cant tend to produce roll rate time histories that are positive or negative over the duration of flight. With a fully reconstructed M matrix, products of angular velocity components can be readily formed:

$$qr = \tfrac{1}{2}(M_{3,2} + M_{2,3}) \tag{20}$$

$$pr = \tfrac{1}{2}(M_{1,3} + M_{3,1}) \tag{21}$$

$$pq = \tfrac{1}{2}(M_{2,1} + M_{1,2}) \tag{22}$$

For example, if the roll rate algebraic sign is known to be positive at some time instant from an external sensor and the sum of $M_{12} + M_{21}$ is negative, then sign(q) must be negative. This logic can be used to establish the algebraic sign of the yaw rate as well. When the minimum set of three triaxial accelerometers is employed in a sensor cluster, if sign($\tilde{p}$) is known, then sign($\tilde{q}$) can be inferred and visa versa. However, sign($\tilde{r}$) must be established independently.

If the algebraic sign of select components of angular velocity are not known then previous recent states of the body can be used to estimate the algebraic sign at a particular time instant. Denote x_p, x_q, and x_r as sequences of recent previous values of p, q, and r, respectively. Furthermore, denote δx_p, δx_q, and δx_r as the maximum expected change of p, q, and r during a given time interval. If sign[max(x_p) + δx_p] = sign[(min(x_p) − δx_p], then the algebraic sign of x_p is assumed to be the algebraic sign of p. Similar arguments apply to q and r. This technique must be initialized with the correct algebraic sign and can fail to predict an algebraic sign estimate if all components of angular velocity are near zero. Once this condition is encountered, the algebraic signs must be reset by an external means. Other techniques based on numerically integrating the angular acceleration estimates can also be utilized. These methods have the disadvantage of occasionally incorrectly predicting the algebraic sign when crossing through zero and subsequently lock-in on the incorrect algebraic sign.

Measurement Error Sensitivity Analysis

To evaluate how acceleration measurement errors map into errors in angular velocity and angular acceleration, error propagation for a sensor cluster consisting of three triaxial acceleration sensors is considered. Noisy acceleration signals induce two distinct types of errors, namely, errors in the magnitude of the angular rate and acceleration components, as well as errors in the algebraic sign of the angular rates. Here, we only consider magnitude errors. Each acceleration measurement contains noise components. The substitution of the noisy sensor data into the acceleration matrix in Eq. (3) yields an additional error matrix A_N that degrades reconstruction of the M matrix as

$$\begin{bmatrix} \hat{M}_{1,1} & \hat{M}_{1,2} & 0 \\ \hat{M}_{2,1} & \hat{M}_{2,2} & 0 \\ \hat{M}_{3,1} & \hat{M}_{3,2} & 0 \end{bmatrix} = (A + A_N)R^{-1} \tag{23}$$

The term $A_N R^{-1}$ is a function of sensor cluster geometry and sensor noise and is expressed as

$$A_N R^{-1} = \begin{bmatrix} N_{1,1} & N_{1,2} & 0 \\ N_{2,1} & N_{2,2} & 0 \\ N_{3,1} & N_{3,2} & 0 \end{bmatrix} \tag{24}$$

Equation (23) separates the correct estimation of the M matrix from the estimation errors due to sensor noise. The estimated M matrix that includes the effect of sensor noise is

$$\hat{M} = \begin{bmatrix} \hat{M}_{1,1} & \hat{M}_{1,2} & 0 \\ \hat{M}_{2,1} & \hat{M}_{2,2} & 0 \\ \hat{M}_{3,1} & \hat{M}_{3,2} & 0 \end{bmatrix} = \begin{bmatrix} -\tilde{q}^2 - \tilde{r}^2 & -\tilde{\alpha}_Z + \tilde{p}\tilde{q} & 0 \\ \tilde{\alpha}_Z + \tilde{p}\tilde{q} & -\tilde{p}^2 - \tilde{r}^2 & 0 \\ -\tilde{\alpha}_Y + \tilde{p}\tilde{r} & \tilde{\alpha}_X + \tilde{q}\tilde{r} & 0 \end{bmatrix} + \begin{bmatrix} N_{1,1} & N_{1,2} & 0 \\ N_{2,1} & N_{2,2} & 0 \\ N_{3,1} & N_{3,2} & 0 \end{bmatrix} \tag{25}$$

To illustrate the complex manner in which sensor errors affect angular rate estimates, first consider the simplified case where one sensor is located along the $\boldsymbol{J}_B$ axis and the other two sensors are along the $\boldsymbol{I}_B$ axis, one at the nose and one near the tail. In this case, the body axes and computational axes are aligned. To further simplify matters, consider the case where $\dot{p} = \dot{q} = \dot{r} = 0$. By the use of Eq. (25), the estimated angular velocity components in terms of sensor error and the actual angular velocity components is given by Eqs. (26–28):

$$\hat{p} = s_{\hat{p}}\sqrt{\tfrac{1}{2}\left[N_{1,1} - N_{2,2} + \tilde{p}^2 - \tilde{q}^2 + E\right]} \tag{26}$$

$$\hat{q} = s_{\hat{q}}\sqrt{\tfrac{1}{2}\left[-N_{1,1} + N_{2,2} - \tilde{p}^2 + \tilde{q}^2 + E\right]} \tag{27}$$

$$\hat{r} = s_{\hat{r}}\sqrt{\tfrac{1}{2}\left[-N_{1,1} - N_{2,2} + \tilde{p}^2 + \tilde{q}^2 + 2\tilde{r}^2 - E\right]} \tag{28}$$

$$E = \sqrt{\tilde{p}^4 + 2\tilde{p}^2\tilde{q}^2 + \tilde{q}^4 + (N_{1,1} - N_{2,2})^2 + (N_{1,2} + N_{2,1})^2 + 4\tilde{p}\tilde{q}(N_{1,2} + N_{2,1}) + 2(\tilde{p}^2 - \tilde{q}^2)(N_{1,1} - N_{2,2})} \tag{29}$$

The product terms that contain angular rate and sensor error components indicate the interaction between the true angular velocity and the estimation errors. Notice that estimation of pitch rate $\hat{q}$ is not dependent on the actual yaw rate, but the yaw rate estimate does depend on the actual pitch rate. The sensitivity of angular velocity component estimation to acceleration measurement error is a complex function of sensor geometry through the various $N_{i,j}$ terms and the actual angular velocity components.

Now consider a more general setting, where the estimation algorithm given by Eqs. (8–13) is expressed in a compact form:

$$\boldsymbol{Y} = F(\boldsymbol{U}) \tag{30}$$

where the input to the algorithm is the acceleration measurements $\boldsymbol{U}$ and the output of the algorithm is the angular velocity and angular acceleration components $\boldsymbol{Y}$:

$$\boldsymbol{U} = \left[a_{X\varphi}\ \ a_{Y\varphi}\ \ a_{Z\varphi}\ \ a_{X\beta}\ \ a_{Y\beta}\ \ a_{Z\beta}\ \ a_{X\chi}\ \ a_{Y\chi}\ \ a_{Z\chi}\right]^T \tag{31}$$

$$\boldsymbol{Y} = [p\ \ q\ \ r\ \ \alpha_X\ \ \alpha_Y\ \ \alpha_Z]^T \tag{32}$$

We seek to understand how perturbations in the vector $\boldsymbol{U}$, representing sensor error, map into perturbations in the vector $\boldsymbol{Y}$, representing estimation error. Equation (32) can be approximated locally using a Taylor series retaining only the linear term, to provide a relationship between measurement and estimation errors:

$$\delta\boldsymbol{Y} = G \cdot \delta\boldsymbol{U} \tag{33}$$

The matrix G represents the sensitivity of computed angular velocity and acceleration components to errors in the input acceleration data and can be numerically computed using finite differences or analytically evaluated about a given point. The sensitivity matrix G is a nonlinear function of geometric parameters and instantaneous angular rates and acceleration. If each error source is independent and all noise sources have the same rms value, the rms error of the ith output is given by

$$\frac{\text{rms}_{Y_i}}{\text{rms}_U} = \sqrt{\sum_{j=1}^{m} G_{ij}^2} \tag{34}$$

Equation (34) is defined as the rms ratio. The rms values for accelerometer error are known from manufacturer specifications, whereas control system designers prescribe levels of fidelity in estimated angular velocity and acceleration components. To investigate acceleration measurement error propagation through the estimation algorithm, consider a typical direct fire atmospheric rocket that is 150 cm in length and has a diameter of 3.5 cm. Acceleration data are recorded at three points on the rocket. The projectile body axis is defined in the conventional manner such that the $\boldsymbol{i}_B$ axis emanates from the mass center of the projectile and points toward the nose. The $\boldsymbol{j}_B$ and $\boldsymbol{k}_B$ axes form an orthogonal set.

The first geometric configuration considered, denoted the L configuration, comprises a sensor mounted along each body axis. Different sensor configurations are obtained by rotating the sensor cluster about the axis of symmetry of the projectile by the sensor constellation angle θ. In the results to follow, the angular acceleration components are set to zero. Figures 3–8 show the rms ratio for estimated roll, pitch, and yaw rate to acceleration measurement error as a function of the actual roll rate and sensor constellation angle. In Figs. 3–8, the sensor along the axis of symmetry, $\boldsymbol{i}_B$, is located 85 cm from the projectile mass center toward the nose, whereas the sensors along the $\boldsymbol{j}_B$ and $\boldsymbol{k}_B$ axes are located 3.5 cm from the center of rotation. Figures 3–5 show the rms ratio computed for low pitch and yaw rates. When the projectile is rolling slowly, the error sensitivity is greatest because the acceleration noise is a relatively large portion of the total acceleration measurement signal. Figures 6–8 are similar to Figs. 3–5 except the pitch and yaw rates are slightly higher (1 rad/s). The largest error sensitivity occurs when the nominal roll rate is zero. For most constellation angles, the error sensitivity decreases with increasing roll rates. However, Figs. 6–8 also show a nonlinear ridgeline emanating from $p = 0$. The ridgeline of high rms ratio rotates for different nominal pitch and yaw rate values. This error ridgeline is particularly troublesome because projectile pitch and yaw rates are oscillatory in nature. Virtually any combination of pitch and yaw rates is possible at a given instant in time, including pitch and yaw rate combinations in the high error sensitivity ridgeline. Figures 9–11 plot the rms ratio of the estimated yaw rate for the L configuration as a function of the nominal pitch and yaw rates for three different constellation angles with the nominal roll rate equal to 2 rad/s. The rms ratio ridge also rotates with the constellation angle.

Figures 12–14 show the same data as Figs. 6–8 except for the O configuration. The O configuration employs two accelerometers mounted on opposite ends of the $\boldsymbol{k}_B$ axis and one accelerometer on the $\boldsymbol{j}_B$ axis. For Figs. 12–14 the pitch rate is zero and the yaw rate is 1.41 rad/s. Error sensitivity of roll rate is large for low roll rate and rapidly decays as roll rate is increased. When the pitch and yaw rates increased, error sensitivity of q and r is flat for all constellation

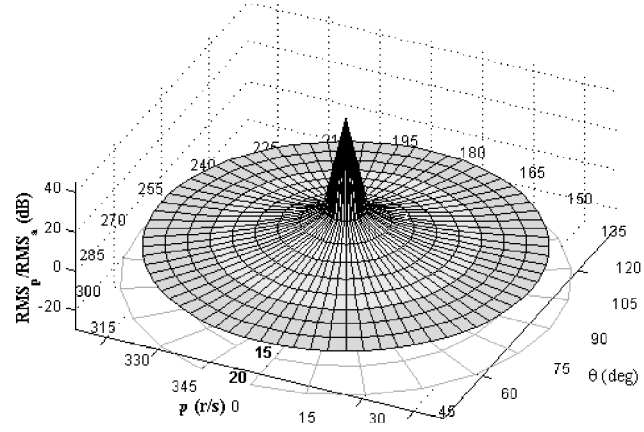

Fig. 3 Estimated projectile roll rate rms ratio of for L configuration vs nominal roll rate and sensor constellation angle: $q = 0.0001$ rad/s, $r = 0.0001$ rad/s.

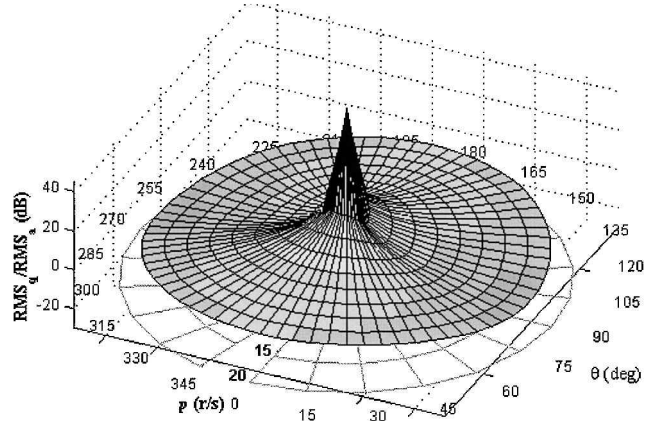

Fig. 4 Estimated projectile pitch rate rms ratio for L configuration vs nominal roll rate and sensor constellation angle: $q = 0.0001$ rad/s, $r = 0.0001$ rad/s.

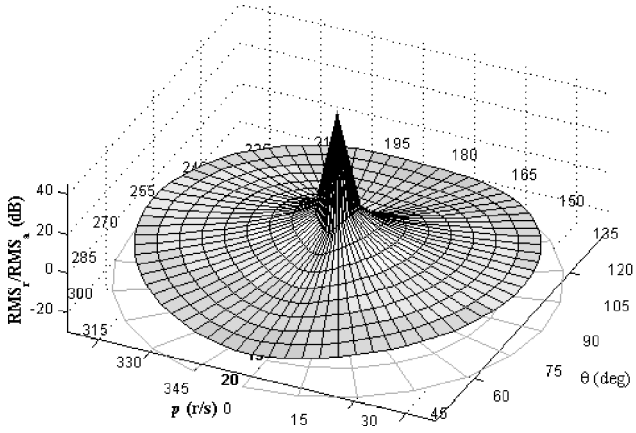

Fig. 5 Estimated projectile yaw rate rms ratio for L configuration vs nominal roll rate and sensor constellation angle: $q = 0.0001$ rad/s, $r = 0.0001$ rad/s.

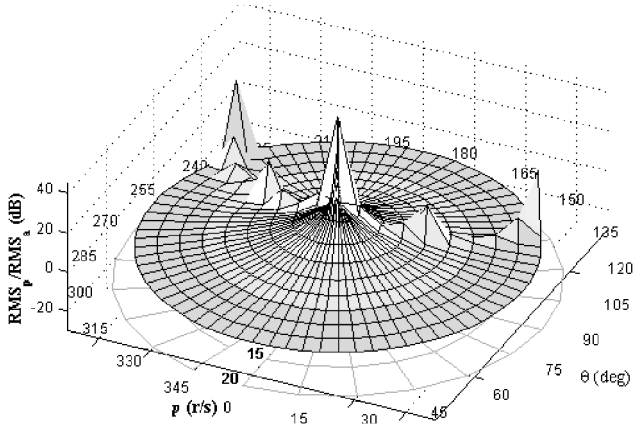

Fig. 6 Estimated projectile roll rate rms ratio for L configuration vs nominal roll rate and sensor constellation angle: $q = 1$ rad/s, $r = 1$ rad/s.

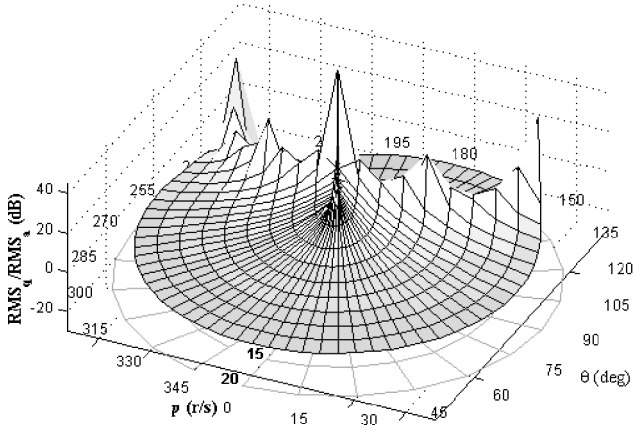

Fig. 7 Estimated projectile pitch rate rms ratio for L configuration vs nominal roll rate and sensor constellation angle: $q = 1$ rad/s, $r = 1$ rad/s.

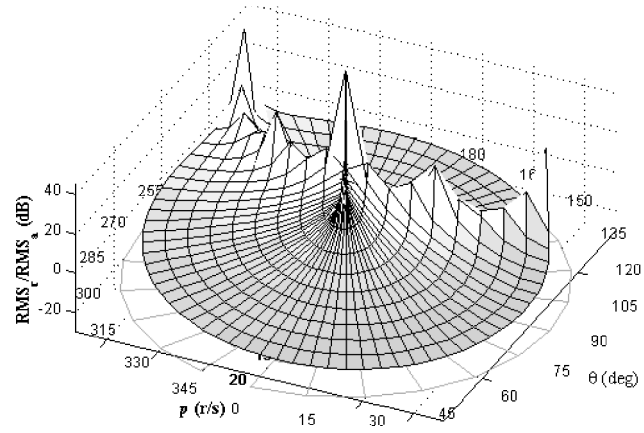

Fig. 8 Estimated projectile yaw rate rms ratio for L configuration vs nominal roll rate and sensor constellation angle: $q = 1$ rad/s, $r = 1$ rad/s.

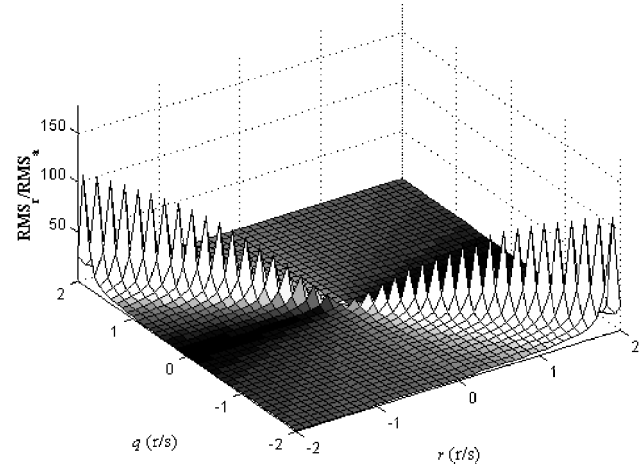

Fig. 9 Estimated yaw rate rms ratio for L configuration vs nominal pitch and yaw rate: $\theta = 0$ deg.

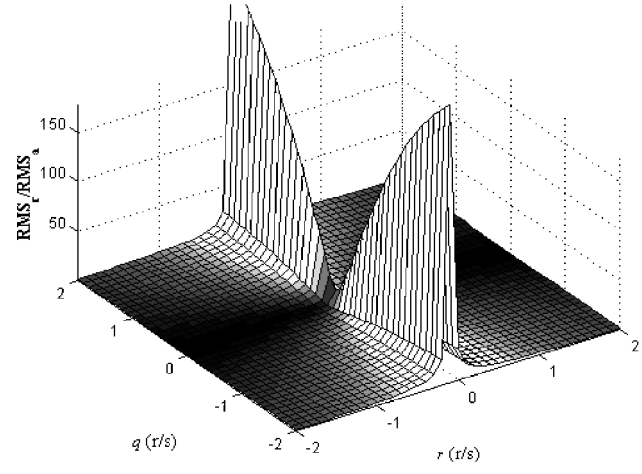

Fig. 10 Estimated yaw rate rms ratio for L configuration vs nominal pitch and yaw rate: $\theta = 45$ deg.

angles and nominal roll rates. The level of this flat region is comparatively higher than the error sensitivity of the configuration L. Note that the estimation algorithm is based on data at a single time instant so that poor angular velocity estimation at one instant does not corrupt future angular velocity estimates.

Skin-Mounted Triaxial Acceleration Measurement Sensor Fusion

The algorithms discussed can be employed to estimate angular rates and acceleration of a projectile with an array of sensors mounted on the skin of the body. The sensor suite is composed of n rings of sensors, with each ring containing m sensors, where the sensors in a ring are equally spaced azimuthally. A schematic is shown in Fig. 15. With a large number of triaxial acceleration measurements available, several different options are possible to fuse the sensor data together. At one extreme, all acceleration measurements are used to estimate the M matrix defined earlier, followed by computation of the angular velocity and acceleration components using Eqs. (14–19). At the other extreme, l groups of three-point measurements are used to calculate l different predictions of the angular velocity and acceleration components using Eqs. (8–13). Median values of the l estimated parameters are used to determine the final

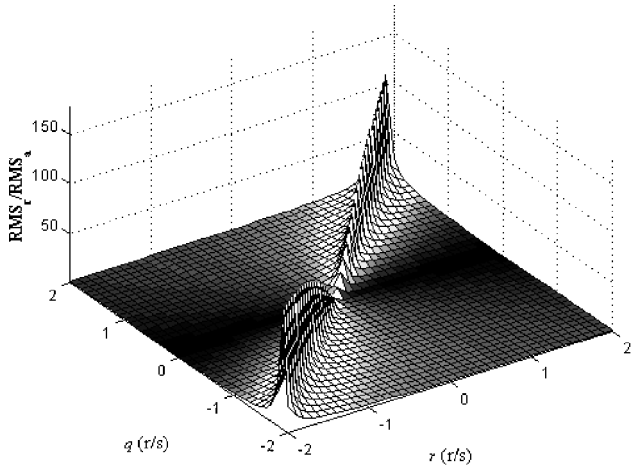

Fig. 11 Estimated yaw rate rms ratio for L configuration vs nominal pitch and yaw rate: $\theta = 90$ deg.

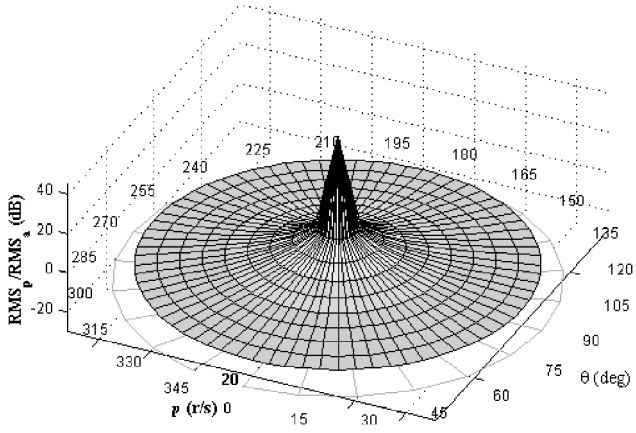

Fig. 12 Estimated roll rate rms ratio for O configuration vs nominal roll rate and sensor constellation angle: $q = 0$ rad/s, $r = 1.414$ rad/s.

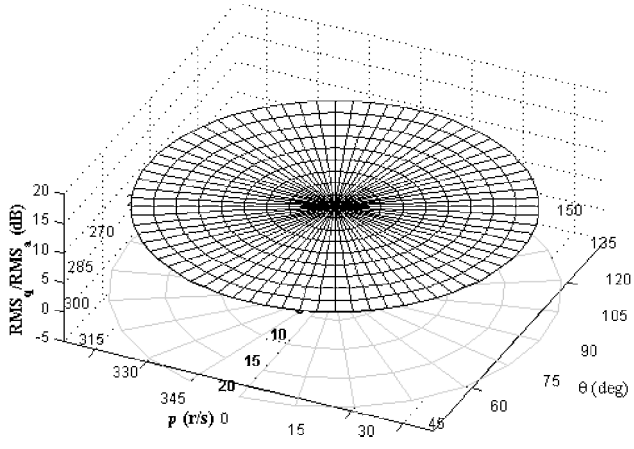

Fig. 13 Estimated pitch rate rms ratio for the O configuration vs nominal roll rate and sensor constellation angle: $q = 0$ rad/s, $r = 1.414$ rad/s.

estimated value for a parameter. The l sensor clusters are randomly selected except for the constraint that the distance matrix R is full rank.

Figures 16–21 provide estimation results for a trajectory of a generic direct fire rocket in atmospheric flight. The rocket trajectory shown in the results to follow has been generated from a six-degrees-of-freedom projectile simulation. Normally distributed random noise, with a standard deviation of 0.031 m/s^2, is added to each acceleration measurement to replicate actual noisy sensors. The signals are also quantized using 64 floating point bytes to account for analog to digital conversion.[13] The algebraic sign of the roll rate is

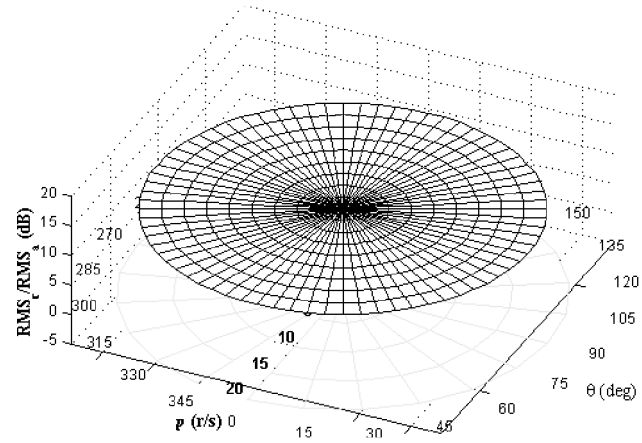

Fig. 14 Estimated yaw rate rms ratio for the T configuration vs roll rate and sensor constellation angle: $q = 0$ rad/s, $r = 1.414$ rad/s.

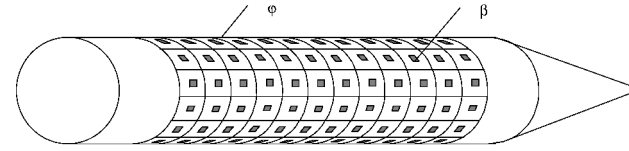

Fig. 15 Acceleration measurement sensor configuration.

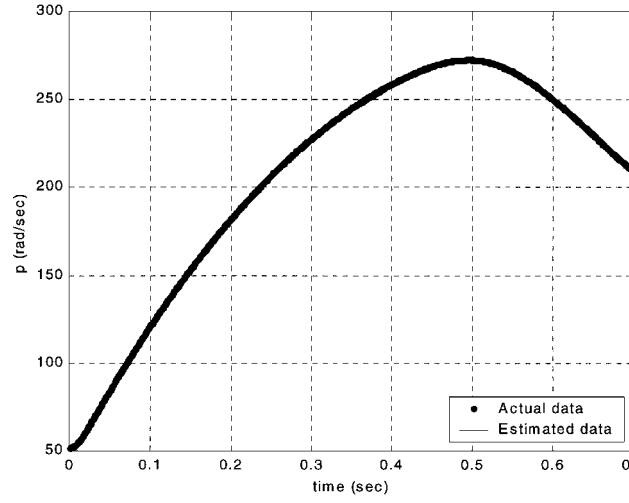

Fig. 16 Actual and estimated roll rate vs time.

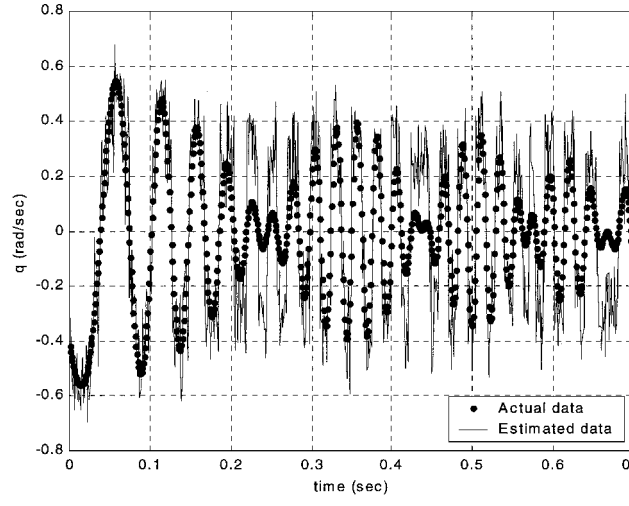

Fig. 17 Actual and estimated pitch rate vs time.

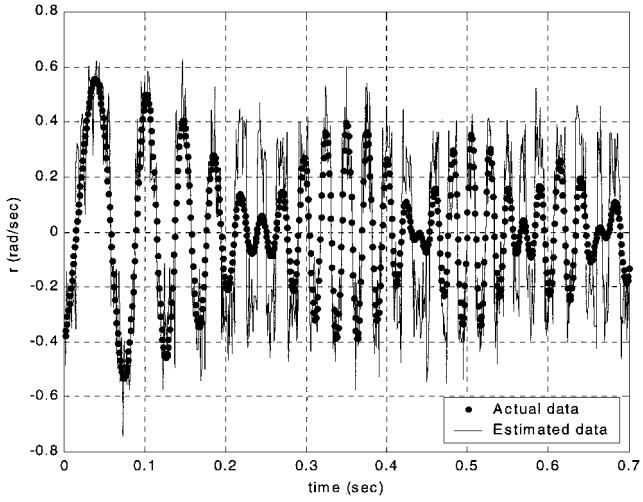

Fig. 18 Actual and estimated yaw rate vs time.

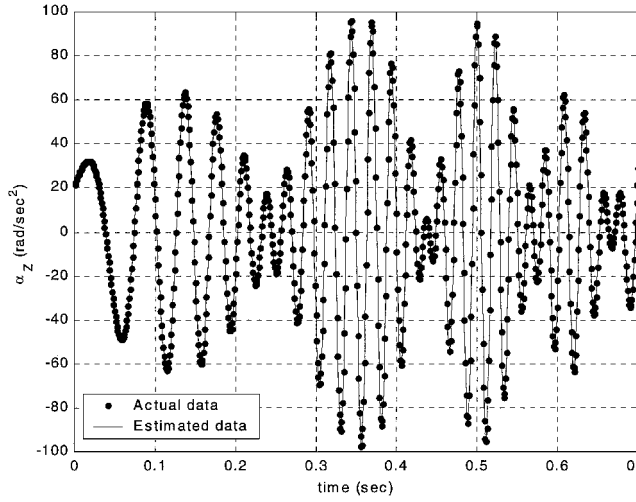

Fig. 21 Actual and estimated yaw acceleration vs time.

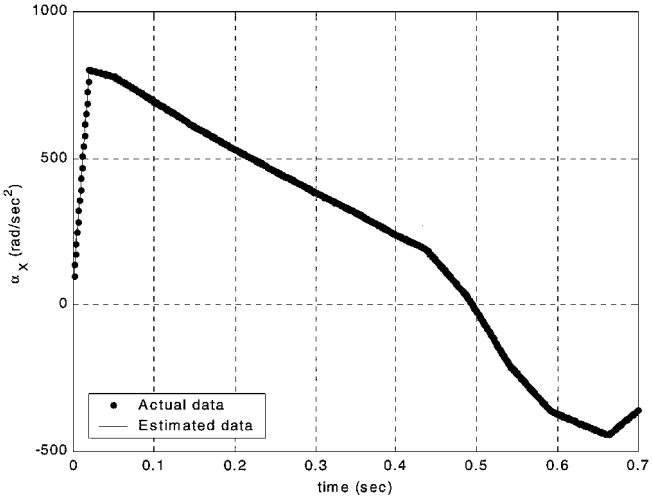

Fig. 19 Actual and estimated roll acceleration vs time.

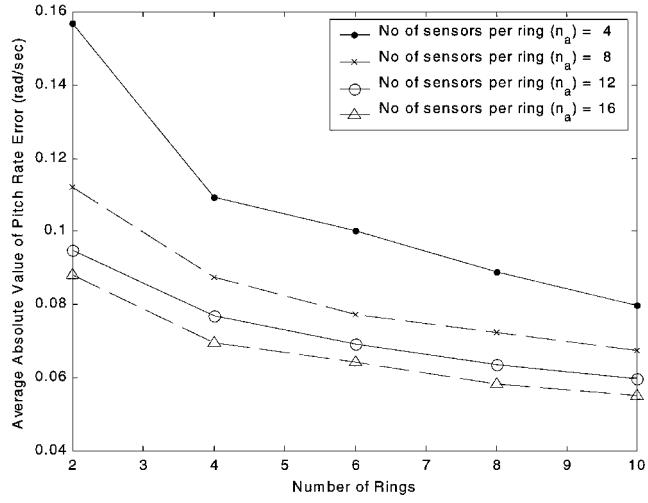

Fig. 22 Average error magnitude vs sensor configuration.

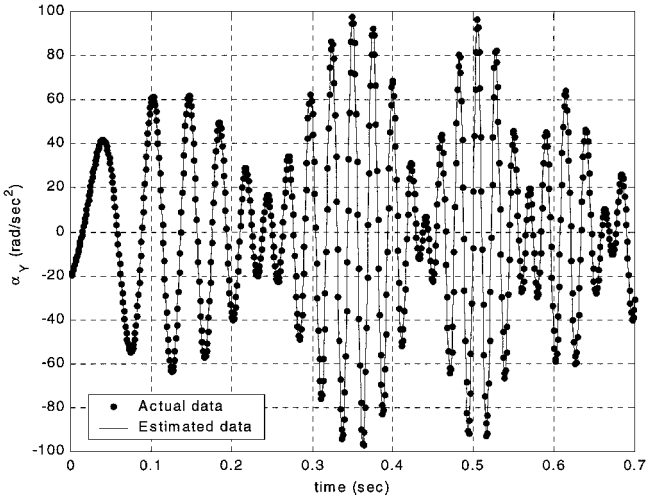

Fig. 20 Actual and estimated pitch acceleration vs time.

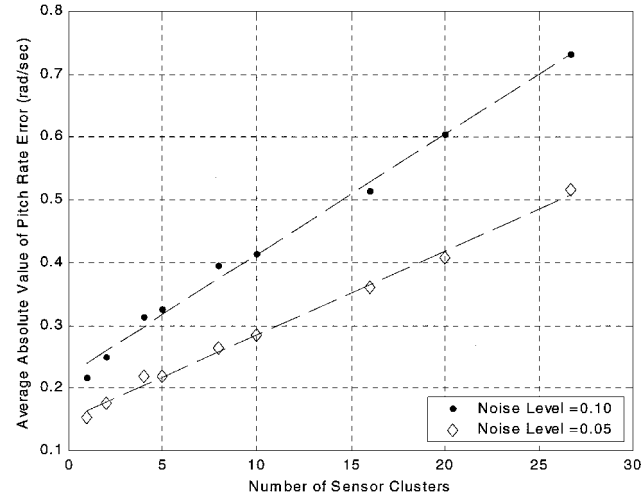

Fig. 23 Average error magnitude vs sensor fusion technique.

generally known for a direct fire rocket. Hence, the angular rates are computed assuming the algebraic sign of roll rate is known. The angular velocity and acceleration components are estimated using a single cluster of 80 triaxial sensors. For this typical example, roll rate and all angular acceleration components are estimated accurately over the entire trajectory in the presence of noise and quantization. However, the pitch and yaw rate estimations are notably less accurate and more sensitive to acceleration measurement error. In particular, when pitch and yaw rate is small, the estimation errors are relatively large. Conversely, when the pitch and yaw rates are largest, the estimation is reasonably accurate.

Figures 22–24 show the errors encountered in estimating pitch rate for different sensor configurations. For Figs. 22–24, the average absolute value of the error between the actual and estimated pitch rate over the entire trajectory is reported. Figure 22 shows the average pitch rate error as a function of the total number of sensors

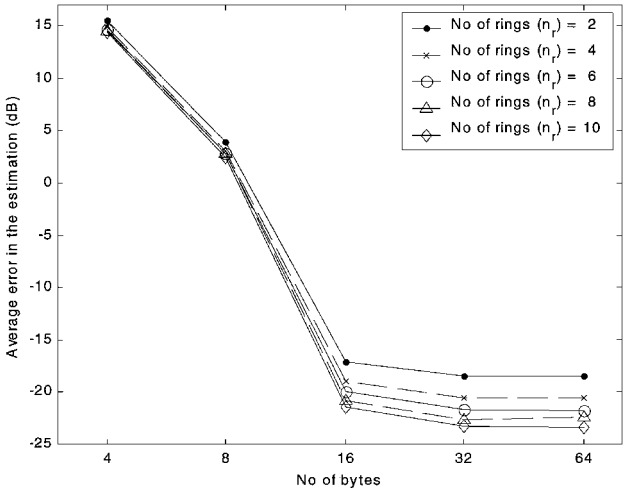

Fig. 24 Average error magnitude vs quantization level.

mounted on the projectile skin. As would be expected, as the number of sensors is increased, either from increasing the number of sensor rings or increasing the number of sensors per ring, pitch rate estimation steadily improves. Figure 23 presents the average pitch rate error vs the number of sensor clusters used in the estimation process. Note that the total number of sensors is held constant in Fig. 23; only the manner in which the sensor data are processed is changed. Figure 23 suggests that the best sensor fusion strategy is one sensor cluster that contains all of the sensors. The minimum error is found by utilizing all of the sensor data to compute the M matrix most accurately. Thus, the estimation algorithm, as given by Eqs. (14–19), tends to magnify errors. Figure 24 plots the average pitch rate error vs the number of bytes used when converting the acceleration measurement data to digital form. The average pitch rate error is a strong function of acceleration measurement quantization. Furthermore, the error reduces sharply until 16 B and then reduces at a lower rate as the number of bytes is further increased. For direct fire rocket applications, acceleration quantization should be performed at no less than 16 B.

Conclusions

The inverse problem of calculating the angular velocity and acceleration of a rigid body using translational acceleration data at three or more points on a body has been given. Two solutions exist for the angular velocity components, differing only in algebraic sign. The error sensitivity of the algorithm described is a nonlinear function of the angular velocity and acceleration components. For the example configuration considered, error sensitivity of roll rate is generally highest at low values of roll rate and rapidly decays as roll rate is increased. For a body that nutates and precesses as it rolls, an error ridge of large error sensitivity is present. The error ridge characteristic can present a problem for the described algorithm when employed on a rigid body where pitch and yaw rates oscillate. In this case, an unfortunate combination of q and r on the ridge will induce large errors. When acceleration is recorded on the skin of an atmospheric rocket, the angular velocity and acceleration components can be effectively estimated. The most effective method to fuse the data is using one cluster that contains all of the sensors. Care must be taken in analog to digital conversion of acceleration measurement, and for direct fire rocket applications, at least 16 B of resolution should be retained.

References

[1]Davis, B., Harkins, T., and Burke, L., "Flight-Test Results of Miniature, Low-Cost, Spin, Accelerometer, and Yaw Sensors," AIAA Paper 97-0422, 1997.

[2]D'Amico, W., "Revolutionary Technologies for Miniature Measurement Systems: Applications to Ground Testing," AIAA Paper 98-0234, 1998.

[3]Davis, B. S., "Using Low Cost MEMS Accelerometers and Gyroscopes as Strapdown IMUs on Rolling Projectiles," *Proceeding of the 1998 IEEE Position, Location, and Navigation Symposium*, Vol. 1, No. 1, Inst. of Electrical and Electronics Engineers, New York, 1996, pp. 594–601.

[4]Costello, M., "Extended Range of a Gun Launched Smart Projectile Using Controllable Canards," *Shock and Vibration*, Vol. 8, 2001, pp. 1–11.

[5]Harkins, T. E., and Brown, T. G., "Using Active Damping as a Precision-Enhancing Technology for 2.75-Inch Rockets," U.S. Army Research Lab., Rept. ARL-TR-1772, Aberdeen Proving Ground, MD, 1999.

[6]Harkins, T. E., "Potential Accuracy Improvements of Inventory Artillery Projectiles Using NATO-Compatible Dragster Fuse," U.S. Army Research Lab., Rept. ARL-MR-438, Aberdeen Proving Ground, MD, 1999.

[7]Ginsberg, J. H., *Advanced Engineering Dynamics*, Cambridge Univ. Press, New York, 1995, pp. 85–89.

[8]Padgaonkar, A. J., Krieger, K. W., and King, A. I., "Measurement of Angular Acceleration of a Rigid Body Using Linear Accelerometers," *Journal of Applied Mechanics*, Vol. 42, Ser. E, No. 3, 1975, pp. 552–556.

[9]Genin, J., Hong, J., and Xu, W., "Accelerometer Placement for Angular Velocity Determination," *Journal of Dynamic Systems, Measurement and Control*, Vol. 119, No. 3, 1997, pp. 474–477.

[10]Harkins, T. E., and Brown, T. G., "Practicability Issues in Deriving Angular Rates From Accelerometer Data for the 2.75-Inch MK66 Rocket," U.S. Army Research Lab., Rept. ARL-MR-392, Aberdeen Proving Ground, MD, 1998.

[11]Angeles, J., *Fundamentals of Robotic Mechanical System*, Springer-Verlag, New York, 1997, pp. 275–288.

[12]Nusholtz, G. S., "Geometric Methods in Determining Rigid Body Dynamics," *Experimental Mechanics*, Vol. 33, No. 2, 1993, pp. 153–158.

[13]Stoer, J., Bulirsh, R., *Introduction to Numerical Analysis*, Springer-Verlag, New York, 1992.

P. Weinacht
Associate Editor